Investigation of electronic structure and thermodynamic properties of quaternary Li-containing chalcogenide diamond-like semiconductors

2016 Semicond. Sci. Technol. 31 125015

(http://iopscience.iop.org/0268-1242/31/12/125015)

IOP Publishing Semiconductor Science and Technology
Semicond. Sci. Technol. 31 (2016) 125015 (18pp) doi:10.1088/0268-1242/31/12/125015

Investigation of electronic structure and thermodynamic properties of quaternary Li-containing chalcogenide diamond-like semiconductors

K Berarma[1], Z Charifi[2], F Soyalp[3], H Baaziz[2], G Uğur[4] and Ş Uğur[4]

[1] Department of chemistry, Faculty of Science, University of M'sila, 28000 M'sila, Algeria
[2] Department of Physics, Faculty of Science, University of M'sila, 28000 M'sila, Algeria
[3] Yüzüncü Yıl University, Faculty of Education, Department of Physics, Van 65080, Turkey
[4] Department of Physics, Faculty of Science, Gazi University 06500 Ankara, Turkey

E-mail: charifizoulikha@gmail.com

Received 25 April 2016, revised 18 September 2016
Accepted for publication 4 October 2016
Published 11 November 2016

Abstract

Using first-principles calculations based on density functional theory, the structural, electronic and thermodynamic properties of Li_2CdGeS_4 and Li_2CdSnS_4 compounds are investigated. We confirmed that both Li_2CdGeS_4 and Li_2CdSnS_4 are diamond-like semiconductors of the wurtz-stannite structure type based on that of diamond in terms of tetrahedra volume. All the tetrahedra are almost regular with major distortion from the ideal occurring in the LiS_4 tetrahedron, with values for S-Li-S ranging from 105.69° to 112.84° in the Li_2CdGeS_4 compound. Furthermore, the Cd-S bond possesses a stronger covalent bonding strength than the Li/Ge-S bonds. In addition, the inter-distances in Li_2CdSnS_4 show a larger spread than the distances in the Li_2CdGeS_4 compound. The electronic structures have been calculated to understand the bonding mechanism in quaternary Li-containing chalcogenide diamond-like semiconductors. Our results show that Li_2CdGeS_4 and Li_2CdSnS_4 are semiconductors with a direct band gap of 2.79 and 2.42 eV and exhibit mixed ionic-covalent bonding. It is also noted that replacing Ge by Sn leads to a decrease in the band gap; this behavior is explained in terms of bond lengths and electronegativity differences between atoms. Optical properties, including the dielectric function, reflectivity, and absorption coefficient, each as a function of photon energy are calculated and show an optical anisotropy for Li_2CdGeS_4 and Li_2CdSnS_4. The static dielectric constant $\varepsilon_1(0)$ and static refractive index $n(0)$ decrease when Ge is replaced by Sn. The influence of pressures and temperatures on the thermodynamic properties like the specific heat at constant volume C_v, and at constant pressure C_p, the Debye temperature Θ_D, the entropy S and the Grüneisen parameter γ have been predicted at enlarged pressure and temperature ranges. The principal aspect from the obtained results is the close similarity of both compounds.

Keywords: semiconductors, *ab initio* calculations, crystal structure, electronic structure, thermodynamic properties, dielectric function

(Some figures may appear in colour only in the online journal)

1. Introduction

Materials known as diamond-like semiconductors (DLSs) are one class of semiconductors that have received increased attention for their promising physical properties. These compounds are attractive materials in the areas of lithium ionic conductors [1], solar cells absorbers [2–6], optoelectrics and second harmonic generation response (SHG) [7–9],

thermoelectric conversion [8–13], spintronics [14] and light emitting diodes [15]. Recently, many studies have been conducted on binary and ternary DLSs; some of the more well-known ternary DLSs are $CuInSe_2$, $CuGaSe_2$, $CuInS_2$, and $CuGaS_2$ crystals. Solid solutions of these compounds are among the best-known photovoltaic materials, however, associated quaternary DLSs have not attracted as much interest most likely due to the difficulty involved in the synthesis of these compounds. Quaternary DLSs should have almost identical properties and the possibility of physical property adjustment has to be increased as the degree of cationic substitution increases.

Previous studies have been done on copper-containing quaternary DLSs compounds such as Cu_2FeSnS_4, Cu_2CdGeS_4 and Cu_2-II-IV-S_4 (Se_4) (II=Fe, Co,Mn, Ni, Zn, Hg, Cd, and IV=Sn, Ge, Si) [16–22]. Most of this early research focused on synthesis and structural characterization. Magnetic measurements of Cu_2MnSnS_4 and new Ag-containing compounds, such as Ag_2CdSnS_4 and Ag_2CdGeS_4 [13–16] have been reported. According to optical measurements, Li_2CdGeS_4 has a direct band gap of 3.15 eV. The electronic structure calculations confirm the existence of this direct gap. The impact of two-photon absorption on second harmonic generation (SHG) in Li_2CdGeS_4 was studied under a typical picosecond excitation (1064 nm). These studies indicate that Li_2CdGeS_4 greatly surpasses the standard $AgGaSe_2$ from the perspective of the IR-generation efficiency in a conventional difference frequency generation scheme [3]. It is found that the replacement of silver or copper with lithium in DLSs having the chemical formula I_2-II-IV-VI4 broadens the band gap in these compounds, increasing their potential in SHG applications due to the possibility of increased laser damage thresholds [23].

Li *et al* investigated the elastic and thermal properties of Li_2CdGeS_4 material under pressure. It is reported that Li_2CdGeS_4 is a direct ductile semiconductor with an energy gap (Γ–Γ) of about 2.42 eV. The latter transforms to the indirect energy gap (along Γ–X point) at about 4 GPa [24]. The synthesis and characterization of Li_2CdSnS_4, Na_2CdSnS_4 and $Na_6CdSn_4s_{12}$ compounds [25] and their crystal structures have been identified by single crystal x-ray diffraction investigations. The semiconductors Li_2CdGeS_4 and Li_2CdSnS_4 were synthesized by Lekse *et al* and their band gaps were measured experimentally to be 3.10 and 3.26 eV for Li_2CdGeS_4 and Li_2CdSnS_4, respectively [26]. Due to the cation ordering, different phases of Ag_2CdGeS_4 have been synthesized for the quaternary alloy Ag_2CdGeS_4 with two-group symmetry; two type in $Pna2_1$, the other in $Pmn2_1$. A study by Lei Wei *et al* shows that the cation arrangement affects their lattice dynamic and electronic properties like bonding strength, band structure as well as their infrared spectrum [27]. The compound Ag_2CdSnS_4 was also confirmed experimentally to exist in the orthorhombic phase (space group *Cmc*21) by Parasyuk *et al* [28]. The value of the energy gap has been estimated to be 2.05 eV at 290 K from the analysis of light absorption spectra, and the temperature dependences of the specific conductivity of Cu_2CdGeS_4 single crystals have been investigated [29].

The quaternary diamond-like semiconductor Ag_2ZnSiS_4 has been synthesized in the monoclinic phase. Electronic band structure calculations reported by Brunetta *et al* show that the compound is a semiconductor with a direct energy gap of 1.88 eV, which is suitable for applications in optoelectronic devices [30]. The phase diagram of the CuGeSe–ZnSe system was investigated by Parasyuk *et al* where the stannite phase of the CuZnGeSe material was confirmed by x-ray powder diffraction [22].

A search for new material is still necessary to find second harmonic generation response compounds and high lithium ionic conducting crystalline compounds. Just a few materials have been investigated previously in solids containing S and Li such as Li_2CdGeS_4 [3, 24, 26] and Li_2CdSnS_4; Na_2CdSnS_4 and $Na_6CdSn_4s_{12}$ [26, 27] were reported to have a large band gap. The ionic conductivity in Li_2ZnGeS_4 [1] was studied and the band gap energy measurements in Li_2CdSnS_4 [25] were done.

Quaternary diamond-like semiconductors Li_2CdGeS_4 and Li_2CdSnS_4 have been found to have a wide band gap, which causes them to have a high laser damage threshold [26, 31]. In these materials, the orientation of the tetrahedral building blocks causes these materials to have a non-centrosymmetric structure, resulting in the loss of inversion symmetry which in turn gives a non-zero second harmonic generation (SHG). The presence of polarizable M-S bonds in these materials results in a strong SHG. Therefore, having a high laser damage threshold and strong SHG makes these materials promising candidates for nonlinear applications in the IR region [26, 31]. It has been found that Li_2CdGeS_4 exhibits higher SHG than that of Li_2CdSnS_4.

Despite the few studies on the structural and electronic properties of these compounds at ambient and high pressure conditions, the thermodynamical properties at finite temperature are quite poorly known. In order to gain a better understanding of the physical properties of Li-containing DLSs compounds, in this study, we report the crystal structure, electronic band structure and density of states (DOS), optical properties of Li_2CdGeS_4 and Li_2CdSnS_4 DLSs, as well as the thermodynamic properties.

In section 2,we give a brief description of the theoretical computational methods. The results discussed in this paper are obtained using density-functional theory (DFT) and are presented in sections 3.1, 3.2, 3.3 and 3.4 respectively. Our ground-state, zero-temperature results for Li_2CdGeS_4 and Li_2CdSnS_4 are displayed in section 3, the crystal structure of Li_2CdGeS_4, Li_2CdSnS_4 compounds and their bonds are described in section 3.1, the electronic properties in terms of band structures, density of states in section 3.2. The optical properties in section 3.3. The lattice thermal properties, such as entropy S, thermal expansion α and specific heat at constant volume and pressure C_v; C_p as obtained from the non-equilibrium Gibbs energy are presented in section 3.4 and finally, section 4 summarizes our results.

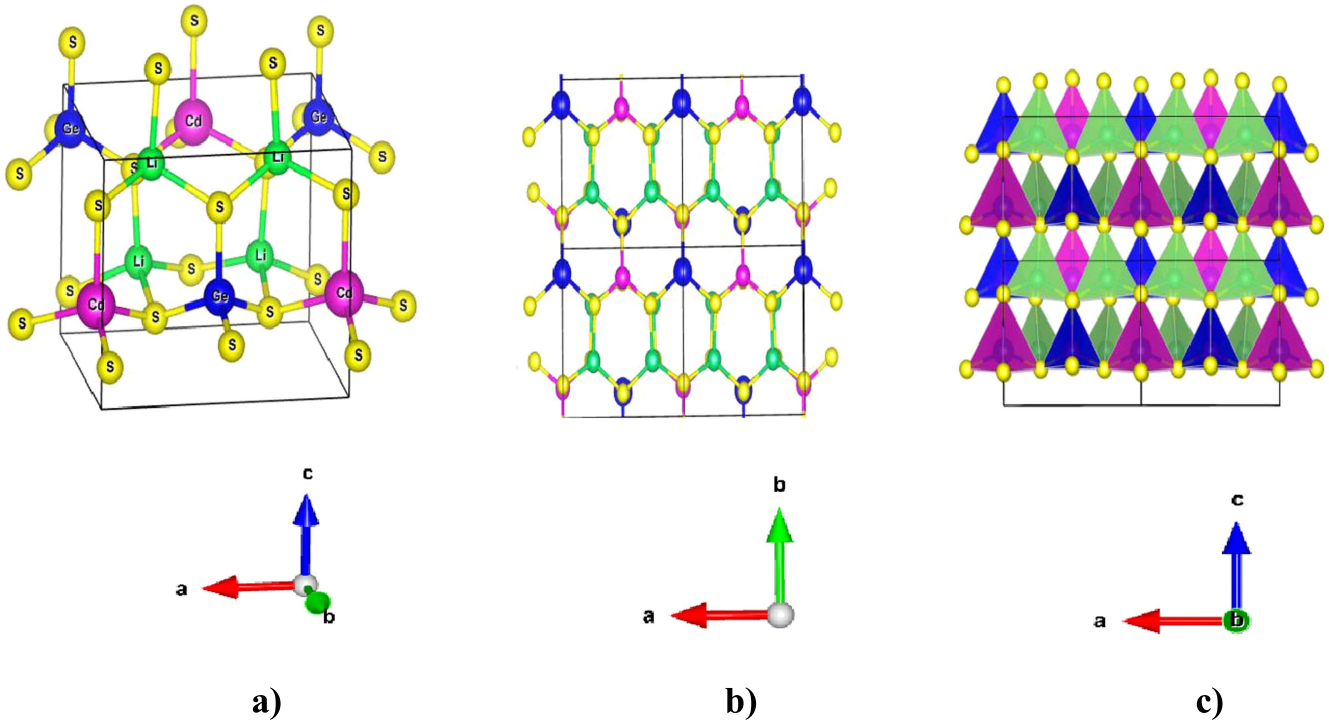

Figure 1. (a) Crystal structure of Li_2CdGeS_4 compound, (b) unit cell diagram of Li_2CdGeS_4 viewed along the *c*-axis. (c) Polyhedral view of Li_2CdGeS_4 extended to show long range cation ordering (green: Li, purple: Cd, blue: Ge/Sn; yellow: S).

2. Computational details and crystal structure of materials

The tetrahedral bonded I_2–II–IV–VI_4 compounds crystallize in non-central-symmetric phases are of benefit for non-linear optics (NLO). Famous quaternary DLSs usually crystallize in one of three space groups: *I*-42*m*, *Pmn*2_1, or *Pna*2_1, with stannite and wurtz-stannite phase types. The *I*-42*m* structure can be obtained from that of cubic diamond while *Pmn*2_1 and *Pna*2_1 are superstructures of hexagonal diamond.

Li_2CdGeS_4 and Li_2CdSnS_4 compounds crystallize in the wurtz-stannite phase (the orthorhombic space group *Pmn*2_1) a non-central-symmetric structures [17], like that of Cu_2CdSiS_4 [32] as shown in figure 1(a). The primitive unit cells of Li_2CdGeS_4 and Li_2CdSnS_4 contain 16 atoms, 2 formulas units per cell. For Li^{1+} ions there is only one unique site and they are aligned in rows down the *c*-axis. Each sulfur anion is tetrahedrally coordinated by two Li cations, one Ge (Sn) cation, and one Cd cation, forming a three-dimensional honeycomb structure. When viewed along the *c* axis, the atoms are aligned in rows in which each cation alternates with the sulfur anions. A projection of the crystal structure is shown in (figure1(b)).

The calculations were carried out using a linearized augmented plane wave full potential scheme (FP-LAPW) within the density-functional theory (DFT) as implemented in the Wien2k package [33]. The exchange–correlation potential was treated within local density approximation (LDA) [34] and generalized gradient approximation (GGA) by Perdew parametrised by Burke and Ernzerhof (PBE) [35]. Furthermore, for the electronic and optical properties we also used the Engel–Vosko (EV–GGA) approach [36] which serves for optimization of the corresponding potential for electronic band structure calculations.

Basis functions, electron density and potential were expanded in spherical harmonics through $l_{\max} = 10$ within non overlapping muffin-tin spheres, and plane waves in the interstitial region. In order to achieve energy eigenvalues convergence, the wavefunctions in interstitial region were expanded in plane waves with a cutoff of $K_{\max} = 8.5/R_{\mathrm{MT}}$ where R_{MT} denotes the smallest atomic sphere radius and $K_{\max}$ gives the magnitude of the largest K vector in the plane-wave expansion. The R_{MT} are taken to be 2, 2.1, 2.3, 2.3 and 1.6 atomic units (a.u) for Li, Cd, Ge, Sn and S respectively. Brillouin-zone (BZ) integrations within the self-consistency cycles were performed via a tetrahedron method [37], using for Li_2CdGeS_4 and Li_2CdSnS_4 48 k points in the IBZ. When the energy difference was less than 0.1 mRy, convergence was assumed. For the calculation of the optical properties, a dense mesh of uniformly distributed k points is required. Hence, the Brillouin zone integration was performed using 720 k points in the IBZ.

The imaginary part '$\varepsilon_2(\omega)$' of the dielectric function can be obtained from the momentum matrix elements between the occupied and unoccupied wavefunctions and is given by [38, 39]:

$$\varepsilon_2(\omega) = \frac{2e^2\pi}{\Omega\varepsilon_0} \sum_{k,V,C} |\langle \Psi_K^c | \hat{u} \times r | \Psi_K^V \rangle^2 | \delta(E_K^c - E_k^V - E) \quad (1)$$

Where Ω is the unit-cell volume, and Ψ_K^c and Ψ_K^V are the conduction band and valence band wave functions at k, respectively. The real part of the dielectric function follows

from the Kramer–Kronig relationship [40]. Furthermore, all the other optical constants of energy dependence, those of refractive index, extinction coefficient, absorption spectrum, reflectivity, and energy loss spectrum can be derived from $\varepsilon_1(\omega)$ and $\varepsilon_2(\omega)$ [41].

$$R(\omega) = \frac{n + \mathrm{i}K - 1}{n + \mathrm{i}K + 1} \tag{2}$$

$$\mathrm{I}(\omega) = \sqrt{2}\,\omega[\sqrt{\varepsilon_1(\omega)^2 + \varepsilon_2(\omega)^2} - \varepsilon_1(\omega)]^{1/2} \tag{3}$$

$$K(\omega) = I(\omega)/2\omega \tag{4}$$

$$n(\omega) = (1/\sqrt{2})[\sqrt{\varepsilon_1(\omega)^2 + \varepsilon_2(\omega)^2} + \varepsilon_1(\omega)]^{1/2} \tag{5}$$

The thermodynamic properties are the basis of solid state science and industrial applications since they can extend our knowledge of the specific behavior of materials under high pressure and high temperature environments. In order to calculate high-T properties, we have employed a quasi-harmonic GIBBS2 code. In this approximation, the non-equilibrium Gibbs energy, given by [42, 43]:

$$\begin{aligned} G^*(x, V; p, T) &= E_{\mathrm{sta}}(x, V) + \mathrm{pV} \\ &\quad + F^*_{\mathrm{vib}}(\mathrm{x}, V; T) + F^*_{\mathrm{el}}(x, V; T) \end{aligned} \tag{6}$$

Where E_{sta} is the static energy (obtained directly from the *ab initio* calculation) and F^*_{vib} is the non-equilibrium vibrational Helmholtz free energy. The crystal structure is completely determined by the volume V, and a number of coordinates, including atomic positions and cell parameters, which we label collectively as x. The electronic free energy is described by F^*_{el}.

At a given pressure (p) and temperature (T), the equilibrium geometry is achieved by minimizing G^* with respect to the remaining variables:

$$G^*(p, T) = \min_{x,V} G^*(x, V; p, T) \tag{7}$$

The minimization of the non-equilibrium Gibbs energy, respect to volume yields the mechanical equilibrium condition:

$$\frac{\partial G^*}{\partial V} = 0 = -p_{\mathrm{sta}} + p - p_{\mathrm{th}} \tag{8}$$

where $p_{\mathrm{sta}} = \mathrm{d}E_{\mathrm{sta}}/\mathrm{d}V$ is the static pressure, $p_{\mathrm{th}} = \partial F^*_{\mathrm{vib}}/\partial V$ the thermal pressure and p is the applied external pressure.

In the quasi-harmonic approximation, the non-equilibrium vibrational Helmholtz free energy is expressed by:

$$F^*_{\mathrm{vib}} = \int_0^\infty \left[\frac{\omega}{2} + k_{\mathrm{B}}T\,\ln(1 - \mathrm{e}^{-\omega/k_{\mathrm{B}}T})\right] g(\omega)\,\mathrm{d}\omega \tag{9}$$

$$F^*(x, V; T) = E_{\mathrm{sta}}(x, V) + F^*_{\mathrm{vib}}(x, V; T) \tag{10}$$

Where $\mathrm{g}(\omega)$ is the phonon density of states (phDOS) and ω is the vibrational frequencies. The phonon density of states approximated by the Debye model is built by treating all phonons as stationary waves in an unstructured solid, and reads:

$$g_{\mathrm{Debye}}(\omega) = \begin{cases} \frac{9n\omega^2}{\omega_{\mathrm{D}}^3} & \text{if } \omega < \omega_{\mathrm{D}} \\ 0 & \text{if } \omega \geqslant \omega_{\mathrm{D}} \end{cases} \tag{11}$$

Where ω_{D} is the Debye frequency, directly related to the Debye temperature:

$$\Theta_{\mathrm{D}} = \frac{\omega_{\mathrm{D}}}{k_{\mathrm{B}}} = \frac{1}{k_{\mathrm{B}}}\left(\frac{6\pi^2 n}{V}\right)^{1/3}\nu_0 \tag{12}$$

In the quasi-harmonic Debye model, Θ_{D} is a function of volume, and the Grüneisen ratio is:

$$\gamma = -\frac{\partial \ln \Theta_{\mathrm{D}}}{\partial \ln V} \tag{13}$$

Inserting g_{Debye} into the quasi-harmonic formulas leads to the following thermodynamic properties (the Helmholtz free energy (F), equilibrium entropy (S), constant-volume heat capacity (C_v) and the thermal expansion coefficient α:

$$\begin{aligned} F &= E_{\mathrm{sta}} + \tfrac{9}{8}nk_{\mathrm{B}}\Theta_{\mathrm{D}} + 3nk_{\mathrm{B}}T\,\ln(1 - \mathrm{e}^{-\Theta_{\mathrm{D}}/T}) \\ &\quad - nk_{\mathrm{B}}TD(\Theta_{\mathrm{D}}/T) \end{aligned} \tag{14}$$

$$S = -3nk_{\mathrm{B}}\ln(1 - \mathrm{e}^{-\Theta_{\mathrm{D}}/T}) + 4nk_{\mathrm{B}}D(\Theta_{\mathrm{D}}/T) \tag{15}$$

$$C_v = 12nk_{\mathrm{B}}D(\Theta_{\mathrm{D}}/T) - \frac{9nk_{\mathrm{B}}\Theta_{\mathrm{D}}/T}{\mathrm{e}^{\Theta_{\mathrm{D}}/T} - 1} \tag{16}$$

$$\alpha = -\frac{1}{V}\left(\frac{\partial V}{\partial T}\right)_P = \frac{\gamma C_v}{VB_T} \tag{17}$$

Where n is the number of atoms per primitive cell, and D represents the Debye integral:

$$D(x) = \frac{3}{x^3}\int_0^x \frac{y^3\mathrm{e}^{-y}}{1 - \mathrm{e}^{-y}}\mathrm{d}y \tag{18}$$

3. Results and discussion

3.1. Determination of the structural and bonding properties

Recently quaternary DLSs show an amplified interest, owing to their technologically useful properties and increased compositional flexibility. The general formula used to represent them is $\mathrm{A^I{}_2B^{II}C^{IV}X_4}$, where the Roman numeral corresponds to the number of valence electrons and the subscript indicates the number of that particular ion in the formula unit.

The total energy of the crystal structures is minimised by varying the volume and relaxing the ionic positions, an equilibrium structure can be reached. The resulting ionic positions, lattice parameters, bulk modulus of LDA as well as data of GGA approximation are presented in table 1 and table 2, and the experimental [26], and theoretical data [23, 24, 44] are also included for comparison. The lattice parameters are in good accordance with those given in [23, 26]. Li_2CdGeS_4 and Li_2CdSnS_4 crystallize in the orthorhombic structure, and Li_2CdGeS_4 compound is predicted to be stable until 8.6 GPa [44]. The magnitude of the bulk modulus B of Li_2CdGeS_4 and Li_2CdSnS_4 quaternary alloys classifies them as easily compressible materials. The

Table 1. Calculated atom positions of Li_2CdGeS_4 and Li_2CdSnS_4 compounds with GGA and LDA approximations.

			GGA			LDA		
Compounds	Atoms	N^a	x	y	z	x	y	z
Li_2CdGeS_4	Li	4(b)	0.7545	0.6701	0.8754	0.7542	0.6695	0.8759
	Cd	2(a)	0	0.8515	0.3719	0	0.8523	0.3718
	Ge	2(a)	0.5	0.8254	0.3749	0.5	0.8278	0.3749
	S1	4(b)	0.7311	0.6637	0.2515	0.7318	0.6680	0.2544
	S2	2(a)	0	0.8614	0.7735	0	0.8619	0.7683
	S3	2(a)	0.5	0.8041	0.7265	0.5	0.8091	0.7251
Li_2CdSnS_4	Li	4(b)	0.7518	0.6695	0.8743	0.7514	0.6697	0.8743
	Cd	2(a)	0	0.8443	0.3734	0	0.8461	0.3741
	Sn	2(a)	0.5	0.8313	0.3751	0.5	0.8348	0.3754

N^a Number of positions and Wyckoff notation.

soft character of these materials arises from the ionic bonding between Li and S.

The diamond-like structure of Li_2CdGeS_4, Li_2CdSnS_4 is an asymmetric unit and it is corner-connected by three types of tetrahedra, LiS_4, CdS_4 and GeS_4 (SnS_4) as can be observed in figure 1(c). The tetrahedra are slightly distorted since the S–M–S (M is Li, Cd, Ge or Sn) angles differ from the regular tetrahedral angle 109.28° (table 3). But generally speaking, the averaged tetrahedral bond angles of S-Li-S, S-Cd-S, S-Ge-S and S-Sn-S are estimated to be about 109° in Li_2CdGeS_4 and Li_2CdSnS_4 compounds which are very close to 109.28°. All the tetrahedra are almost regular with the greatest distortion from ideal arising in the LiS_4 tetrahedron, with the estimated values for S-Li-S range from 105.69° to 112.84° in Li_2CdGeS_4 compound.

The tetrahedral volumes Li-S_4, Cd-S_4, Sn-S_4 and Ge-S_4 are calculated from the bond distances for Li_2CdGeS_4 and Li_2CdSnS_4 using two approximations LDA and GGA. They are found to be 7.26(7.04), 8.80(8.08) and 6.01(5.58) $Å^3$ for Li-S_4, Cd-S_4 and Ge-S_4 and 7.90(7.68), 8.90(8.10), 7.23 (7.01) $Å^3$ for Li-S_4, Cd-S_4 and Sn-S_4 using a GGA(LDA) approximation. It is clearly seen that the volume of all the tetrahedra is increased when we move from the Li_2CdGeS_4 to the Li_2CdSnS_4 compound. The smallest tetrahedra volume is 6.01(5.58) $Å^3$ for Ge-S_4 and the largest is 8.80 (8.08) $Å^3$ for the Cd-S_4 tetrahedra in Li_2CdGeS_4 which show a variation of 2.79 (2.5) $Å^3$. This predicts a hexagonal-derived diamond-like structure which agrees with the Pfitzner's theory [45, 46]. Likewise, Li_2CdSnS_4 also possesses a tetrahedral volume range of 1.67 $Å^3$ (GGA), moreover justifying this hypothesis. Every cation is tetrahedrally coordinated with sulfur anions. It is easy to see that all tetrahedra in Li_2CdGeS_4 and Li_2CdSnS_4 structures are oriented in the same direction along the *c*-axis (see figure 1(c)), thus demonstrating the lack of an inversion center.

The bond lengths for Li-S range from 2.37–2.42 Å (2.39–2.44 Å) in Li_2CdGeS_4 and from 2.43–2.50 Å (2.46–2.52 Å) in Li_2CdSnS_4 using LDA (GGA) approximation respectively (see table 3). The average Li-S bond length in Li_2FeSnS_4 and Li_2FeGeS_4 was found to be 2.43 Å which is similar to our present calculations for the Li_2CdGeS_4 compound.

The average bond length of Ge-S is found to be 2.26 (2.22 Å) which is less than that of the Sn-S bond of 2.44 Å (2.382) using GGA (LDA) respectively. Our estimated bond lengths Ge-S are in good agreement with those measured in Cu_2CdGeS_4 DLSs (with same space group as Li_2CdGeS_4) about 2.28 Å [47]. The inter-distances of the Cd-S bonds average 2.58 Å (2.51 Å) in Li_2CdGeS_4 is in accordance with the same bond lengths found in Li_2CdSnS_4. However it is smaller than the experimental value obtained in Cu_2CdGeS_4 DLSs [47]. The Ge-S, Sn-S and Li-S interatomic distances are slightly smaller than the sum of the respective ionic radii however the bond length Cd-S is found to be greater than the expected value (r (Li^{+1}) = 0.59 Å, r (Cd^{+2}) = 0.97 Å, r (Ge^{4+}) = 0.53 Å, r (Sn^{+4}) = 0.71 Å and r (S^{-2}) = 1.82 Å [11, 48, 49]).

It is noted that replacing Ge by Sn leads to a longer bond length. The Li-S, Cd-S, Ge-S and Sn-S distances in Li_2CdGeS_4 and in Li_2CdSnS_4 are calculated and are compared with the available bond lengths (see table 3). From this table it becomes obvious that the distances in Li_2CdSnS_4 show a larger spread than the distances in the Li_2CdGeS_4 compound.

3.2. Electronic band structures and density of states

The scalar relativistic band structures of Li_2CdGeS_4 and Li_2CdSnS_4 quaternary DLSs compounds along representative symetrical directions of the Brillouin zone were obtained at equilibrium volume from equilibrium within LDA and GGA approximations.

The results showed that LDA and GGA can provide suitable lattice parameters and crystal symmetry for Li_2CdGeS_4 and Li_2CdSnS_4, although an underestimation of the band gap was expected. Thus EV-GGA approximation was also used to calculate the band structures. The Fermi level E_F is shown by a solid horizontal line. The EV-GGA has been demonstrated many times to give band gaps in good agreement with experiments [50, 51].

Because of the similarity of the dispersions of bands using different approximations, we have shown the band structures of Li_2CdGeS_4 and Li_2CdSnS_4 compounds using EV-GGA approximation in figure 2. The gap between the

Table 2. Calculated lattice constants (a, b and c) in Å, bulk modulus (B) in GPa and pressure derivative (B') at equilibrium volume using GGA and LDA compared to experimental and other works Li_2CdGeS_4 and Li_2CdSnS_4 compounds.

	Lattice constants (A°)				B (GPa)			B'(GPa)			Relative Error	
	Present work											
Compounds	GGA	LDA	DFT[23]	Exp [26]	GGA	LDA	DFT[24, 44]	GGA	LDA	DFT[24, 44]	GGA	LDA
Li_2CdGeS_4	a =7.8207	a =7.6642	a =7.601	7.7374	53.87	64.05	57.7 (GGA)	4.33	4.64	4.31 (GGA)	$\left.\frac{\Delta a}{a}\right\|_{Exp} = 1.07$	$\left.\frac{\Delta a}{a}\right\|_{Exp} = -0.94$
							57.4 (LDA)			4.53 (LDA)		
	b = 6.8905	b = 6.7956	b = 6.654	6.8498							$\left.\frac{\Delta b}{b}\right\|_{Exp} = 0.59$	$\left.\frac{\Delta b}{b}\right\|_{Exp} = -0.79$
	c =6.4535	c =6.3282	c = 6.253	6.3688							$\left.\frac{\Delta c}{c}\right\|_{Exp} = 1.32$	$\left.\frac{\Delta c}{c}\right\|_{Exp} = -0.63$
	b/a = 0.881	b/a = 0.886										
	c/a = 0.825	c/a = 0.825										
Li_2CdSnS_4	a = 8.0902	a = 7.9419	a = 7.856	7.9555	49.78	59.40		4.65	4.80		$\left.\frac{\Delta a}{a}\right\|_{Exp} = 1.69$	$\left.\frac{\Delta b}{b}\right\|_{Exp} = 1.68$
	b = 7.0855	b = 7.0117	b = 6.799	6.9684							$\left.\frac{\Delta c}{c}\right\|_{Exp} = 2.69$	$\left.\frac{\Delta a}{a}\right\|_{Exp} = -0.17$
	c = 6.6640	c = 6.5426	c = 6.394	6.4886							$\left.\frac{\Delta b}{b}\right\|_{Exp} = 0.62$	$\left.\frac{\Delta c}{c}\right\|_{Exp} = 0.83$
	b/a = 0.875	b/a = 0.882										
	c/a = 0.823	c/a = 0.823										

Table 3. Selected interatomic distances (Å) and angles (deg) in $Pmn2_1$ crystal structure of Li_2CdGeS_4 and Li_2CdSnS_4 compounds.

Compounds	Atoms	Our calculation		DFT	Experimental [25]
		GGA	LDA		
Li_2CdGeS_4	Li-S1	2.4380	2.4223	2.401 [44]	
	Li-S2	2.4201	2.3917	2.416 [44]	
	Li-S3	2.3953	2.3684	2.422 [44]	
	Li-S4	2.4340	2.4010	2.406 [44]	
	S-Li-S	112.8443	113.134		
	S-Li-S	105.6903	106.7018		
	S-Li-S	108.2697	108.4172		
	S-Li-S	109.8894	108.3074		
	S-Li-S	110.1504	110.1732		
	S-Li-S	109.9030	110.0457		
	Ge-S1(x2)	2.2678	2.2178	2.228 [44]	
	Ge-S2	2.2548	2.2134	2.228 [44]	
	Ge-S3	2.2736	2.2194	2.238 [44]	
	S-Ge-S(x2)	111.5971	111.1805		
	S-Ge-S(x2)	108.5986	108.3838		
	S-Ge-S	105.6923	106.5071		
	S-Ge-S	110.5748	111.0357		
	Cd-S1(x2)	2.5883	2.5181	2.527 [44]	
	Cd-S2	2.5928	2.5096	2.544 [44]	
	Cd-S3	2.5514	2.5096	2.556 [44]	
	S-Cd-S(×2)	110.7668	110.5274		
	S-Cd-S(×2)	108.2550	107.930		
	S-Cd-S	110.0528	110.5021		
Li_2CdSnS_4	S-Cd-S	108.6652	109.3451		
	Li-S1	2.5218	2.5032	2.352-2.382 [23]	2.351(20)
	Li-S2	2.4783	2.4473		2.445(22) × 4
	Li-S3	2.4611	2.4326		2.4247(7)
	Li-S4	2.4977	2.4802		
	S-Li-S	110.6647	110.8996		
	S-Li-S	107.4256	108.3902		
	S-Li-S	108.3931	108.3241		
	S-Li-S	110.2326	109.1186		
	S-Li-S	110.1105	110.0918		
	S-Li-S	109.9635	109.9955		
	Sn-S1(x2)	2.4416	2.3858	2.342-2.346[23]	2.397(9)
	Sn-S2	2.4474	2.3843		2.399(6)
	Sn-S3	2.4322	2.3728		2.406(5) × 4
	S-Sn-S(x2)	111.0682	110.5315		
	S-Sn-S(x2)	108.8479	108.4135		
	S-Sn-S	106.2302	107.4785		
	S-Sn-S	110.6431	111.4072		
	Cd-S(x2)	2.5957	2.5231	2.521-2.537 [23]	2.527(8)
	Cd-S	2.5808	2.4972		2.503
	Cd-S	2.5817	2.4946		2.539(5) × 4
	S-Cd-S(×2)	110.900	110.3762		
	S-Cd-S(×2)	108.5708	108.0931		
	S-Cd-S	107.4135	108.5120		
	S-Cd-S	110.3882	111.2974		

valence and conduction bands is calculated at Γ point within three different approximations, and is compared with the available results in table 4. It can be seen that the compounds under study are large direct band gap semiconductors which is in agreement with previous work [23, 24]. Li *et al* [23] have reported that Li_2CdGeS_4 has an indirect band gap of 2.78 eV calculated using the plane-wave pseudopotential method. In fact, our calculations using three approximations yielded a direct band gap of about 2.79 eV using EV-GGA. Lekse *et al* used diffuse-reflectance spectroscopy to determine band gaps which were of 3.10 and 3.26 eV for Li_2CdGeS_4 and Li_2CdSnS_4, respectively [26]. This result is in contrast to that found by Devi *et al* that the Li_2CdSnS_4 compound does not show any absorption edge [25]. The experimentally estimated

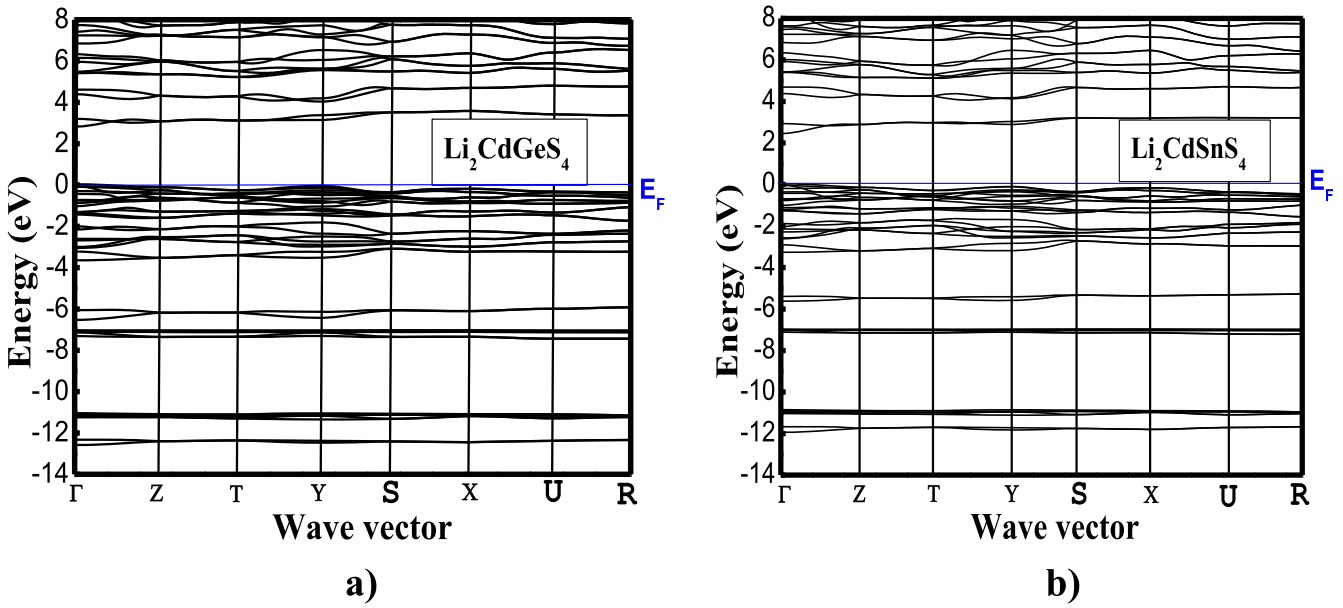

Figure 2. Band structure along the symmetry lines of the Brillouin zone for (a) Li_2CdGeS_4 and (b) Li_2CdSnS_4 diamond-like semiconductors calculated using the EVGGA approach. The position of the Fermi level is shown by the horizontal line.

band gap is 3.10 eV, a deviation of 11% from our calculated value.

The insulating behavior of Li_2CdGeS_4 and Li_2CdSnS_4 materials can be explained as follows: each formula unit, two electrons from two Li atoms fill the S-p orbitals of one S atom and two electrons from Cd-s orbitals fill another S atom. The third and the fourth are filled by electrons from Ge-s and Ge-p, resulting in a complete filling of the valence band (VB) and accordingly the formation of energy gap and an insulating behavior.

It is clear that the GGA and LDA underestimated the band gap, and the estimated values of *Eg* were less than those reported in [26]. The obtained value for *Eg* within EV-GGA is in good agreement with the experimental one compared with that calculated using both LDA and GGA.

It is also noted that replacing Ge by Sn leads to a decrease in the band gap. This behavior is reported in previous works [26] and is also observed in Cu compounds containing Cu_2CdGeS_4 (2.05 eV) [10] and Cu_2CdSnS_4 (1.38 eV) [52]. It is worth noting that the estimated values of the band gaps are 0.54 eV and 0.22 eV for Cu_2ZnSnS_4 and $Cu_2ZnSnSe_4$, respectively [53]. The replacement of copper with lithium broadens the band gap in these compounds.

In order to explain the trend in the theoretically and experimentally obtained band gap energies, electronegativity differences between atoms in the structures were examined. Using Pauling electronegativities [54], we have calculated the electronegativity difference between sulfur and each of the other elements and it is found to be 1.6, 0.89, 0.62 and 0.57 for Li-S, Cd-S, Sn-S and Ge-S respectively. Average electronegativity differences were estimated to be 1.165 and 1.177 for Li_2CdGeS_4 and Li_2CdSnS_4 respectively. The increase of the electronegativity difference from 0.57 for Li-Ge to 0.62 for Li-Sn leads to an increase in the ionic character of the bonding in these materials. As the bonding in these compounds becomes more ionic the band gap energies of the compounds increase which agrees with the experimental trend. This differs from the observed trend in that, theoretically, Li_2CdGeS_4 has the largest band gap energy (present work, 26), with the smallest average electronegativity difference. It should also be noted that the electronegativity differences between both compounds is very small, 0.0125, which could contribute to the discrepancy in the predicted band gap trend. It appears that electronegativity, by itself, is not sufficient to explain the observed trend so bond lenghts were examined again. Average bond distances in both lithium-containing DLSs were calculated and were found to be 2.26, 2.58 and 2.42 Å for Ge-S, Cd-S and Li-S for Li_2CdGeS_4 while for Li_2CdSnS_4, it is 2.44, 2.59 and 2.49 Å for Sn-S, Cd-S and Li-S respectively. It is clearly seen that the bond lengths in Li_2CdGeS_4 are shorter than those of in Li_2CdSnS_4, thus the shorter the bond distance the more overlap exist between atomic orbitals. This overlap results in stronger bonds and an increase in the band gap energy. These observations seem to explain the observed band gap trend.

To fully explain and understand the origin of the trend in band gap energy, in addition to bond distance and electronegativity, we calculated the DOS to see which orbitals contribute to the states around the band gap. The total (TDOS) and partial density of states (PDOS) of Li_2CdGeS_4 and Li_2CdSnS_4 compounds are shown in figure 3. The overall TDOS and PDOS profiles are in good agreement with the previous theoretical calculation. It is clearly shown that the top of the valence band (VB) is mainly originated from Sn/Ge-p and S-p orbitals, while the bottom of the conduction band (CB) consists of Ge/Sn-s and S-p and Cd-s orbitals. It is clearly seen that for both compounds, Li-s states mainly lie in the conduction band. Hybridizations between Ge-4p/Sn-5p and S-3p as well as Cd-5 s and S-3p states are responsible for

Table 4. Calculated Eg, $\varepsilon_1(0)$ and $\boldsymbol{n}$ (**0**) of Li_2CdGeS_4 and Li_2CdSnS_4 compounds within LDA, GGA and EV-GGA.

Compounds	Eg (eV)						$\varepsilon_1(0)$				n (0)		
	GGA	LDA	EVGGA	Exp	Other works		GGA	LDA	EVGGA		GGA	LDA	EVGGA
Li_2CdGeS_4	2.18	2.19	2.79	3.10 [26]	2.81 [44]	ε_{1xx}	5.513	5.734	4.592	n_{xx}	2.339	2.398	2.141
						ε_{1yy}	5.424	5.618	4.592	n_{yy}	2.335	2.366	2.136
						ε_{1zz}	5.480	5.688	4.592	n_{zz}	2.352	2.389	2.141
Li_2CdSnS_4	1.85	1.86	2.42	3.26 [26]	2.50 [23]	ε_{1xx}	5.3535	5.616	4.509	n_{xx}	2.319	2.011	2.123
						ε_{1yy}	5.3737	5.525	4.565	n_{yy}	2.328	2.017	2.133
						ε_{1zz}	5.4242	5.616	4.565	n_{zz}	2.333	2.018	2.123

the σ bonding states in the upper valence bands and σ^* antibonding states in the conduction bands.

For both compounds, Li-s electronic states mainly lie in the energy range above 2.5 eV with a small contribution in the upper valence band. This indicates that the Li occurs as ions provide charge balance to the $[CdGeS_4]^{-2}$ polyanion in Li_2CdGeS_4 and $[CdSnS_4]^{-2}$ polyanion in Li_2CdSnS_4, and, consequently, the electrostatic interactions between the Li atoms and polyanions contribute to the stability of the structures.

It is clear that the Cd orbitals have a insignificant contribution to CB maximum and VB minimum. The bands located at −10 to −5 eV are isolated ones with strong Cd-d and Ge-s/Sn-s characters. It has been noticed that Ge-s, and S-s/p orbitals have an insignificant influence in the matter of peak heights while replacing Ge by Sn, as shown in figures 3(e)–(f) and (i)–(j). Whereas a significant influence can be seen in the matter of peak heights for Cd-d, and Li-2 s orbitals, as shown in figures 3(e)–(h) and (c)–(d). It is interesting to see that the contribution of Cd and Li-atoms is significantly influenced by substituting Ge by Sn (figures 3(c)–(d) and (g)–(h)), while S-atoms show only minor changes (figures 3(i)–(j)). It is important to see here that the main differences between the considered DLSs are related to the substitution of Sn by Ge atoms. It is obvious to see that almost of the described peaks have increased in height.

To determine the dominance of either covalent or ionic bonding, and according to the calculated electronegativity difference M-S elements, we find an ionic-like bonding picture of the Li–S bonds. The Ge–S bonds show a distinct degree of covalence, while the Cd–S bonds show weaker covalence. Therefore, it concluded that the bonding behavior of Li_2GeCdS_4 is a coexistence of ionic and covalent nature. Furthermore, the Cd-S bond possessed a stronger covalent bonding strength than the Li/Ge-S bonds. In the bonding, the main role is played by Sn/Ge atoms where a charge transfer to Sulfur atoms was observed.

3.3. Optical properties

The linear optical properties are determined by the complex dielectric function $\varepsilon(\omega) = \varepsilon_1(\omega) + i\varepsilon_2(\omega)$ describing the polarization response of the system to an external electromagnetic field with a small wavevector. The electric field of the photon leads to the transition between the occupied and unoccupied states, including plasmons and single particle excitations. The excitation spectra can be described as a joint density of states between the valence and conduction bands. The intraband transition cannot be considered because it is crucial only for metals. We also neglect the indirect interband transitions involving scattering of phonons assuming that they give a small contribution to the frequency-dependent dielectric functions. Li_2CdGeS_4 and Li_2CdSnS_4 crystallize in orthorhombic symmetry, so it has three main dielectric tensors, $\varepsilon_2^{xx}(\omega)$, $\varepsilon_2^{yy}(\omega)$ and $\varepsilon_2^{zz}(\omega)$ components correspond to the electric field $\vec{E}$ being along a, b, and c-crystallographic axes.

The imaginary part of the linear optical properties $\varepsilon_2^{xx}(\omega)$, $\varepsilon_2^{yy}(\omega)$ and $\varepsilon_2^{zz}(\omega)$ for the orthorhombic system (Li_2CdGeS_4 and Li_2CdSnS_4) is calculated and presented in figures 4(a) and (b). The spectral structure of Li_2CdGeS_4 and Li_2CdSnS_4 exhibits three main peaks in $\varepsilon_2^{xx}(\omega)$, $\varepsilon_2^{yy}(\omega)$ and $\varepsilon_2^{zz}(\omega)$ components with small several humps situated on the left and right shoulders. In addition, the maximum peaks are found in between 4.0 eV and 8.0 eV.

The absorption edges occur at 3.10 eV (Li_2CdGeS_4) and 3.23 eV (Li_2CdSnS_4), as shown in figures 4(a) and (b). These absorption edges are originated from the optical transitions between S-3p and Ge-4s/4p (Sn-5s/5p) and Cd-5s/4p states. The optical transitions are calculated from the momentum matrix elements between the occupied and unoccupied bands.

The real part of the dielectric function is obtained from the imaginary part $\varepsilon_2(\omega)$ by means of the Kramers–Kronig transformation [40] as shown in figures 4(c)–(d). From figure 4, we can see a large anisotropy in the real part $\varepsilon_1(\omega)$ of the dielectric function $\varepsilon_1^{xx}(\omega)$, $\varepsilon_1^{yy}(\omega)$ and $\varepsilon_1^{zz}(\omega)$ for Li_2CdGeS_4 and Li_2CdSnS_4. The computed static dielectric constants $\varepsilon_1(0)$ are displayed in table 4. Li_2CdGeS_4 shows a larger high-frequency dielectric constant calculated using different approximations than that of the Li_2CdSnS_4 compound.

The absorption coefficient represents the linear optical response from the valence bands to the lowest conduction bands. Since the absorption is obtained directly from the dielectric function, similarities in the polarization response for

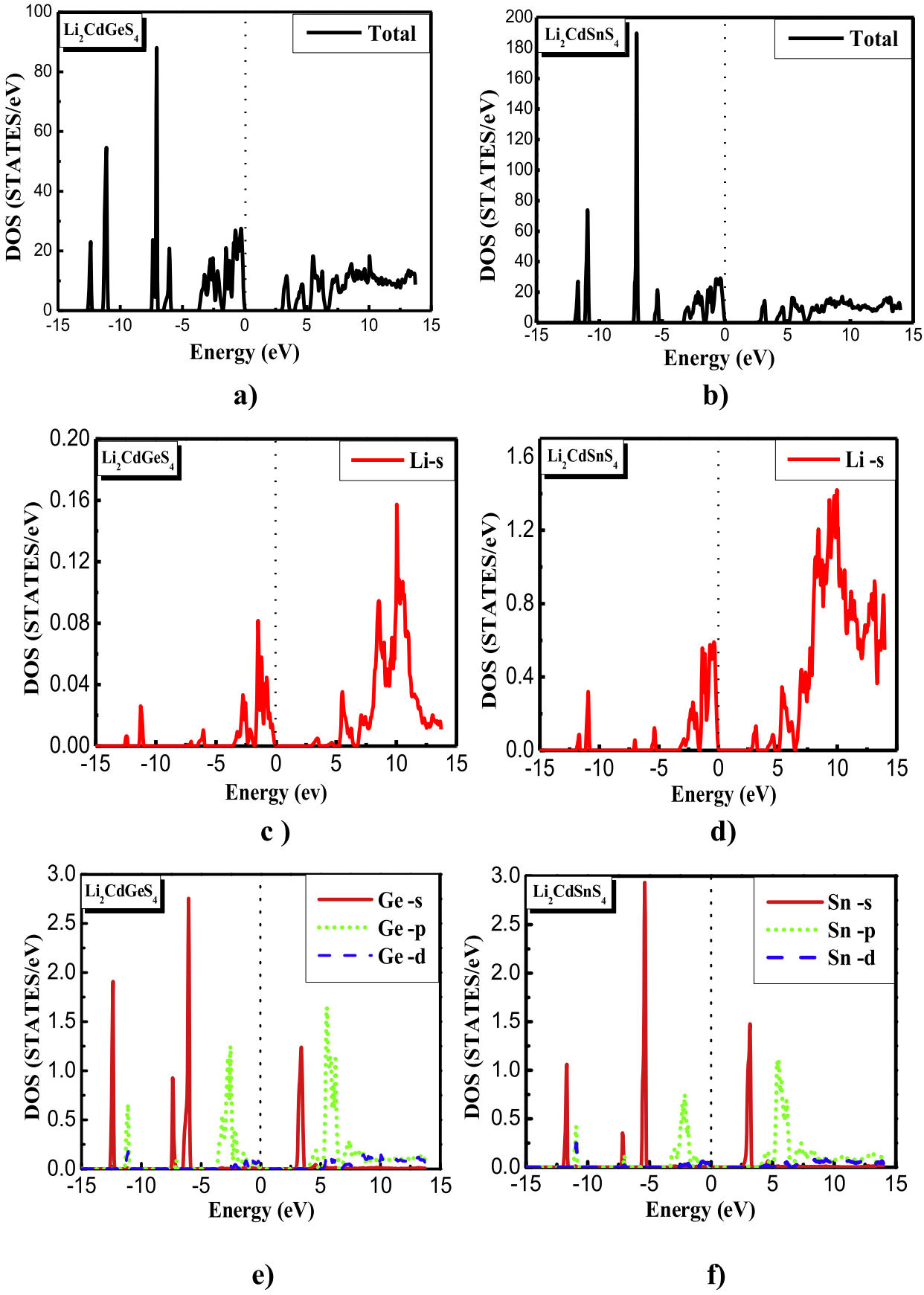

Figure 3. The calculated total and partial density of states for Li_2CdGeS_4 and Li_2CdSnS_4 diamond-like semiconductors. The graph is scaled for 0 eV at the Fermi level (E_F).

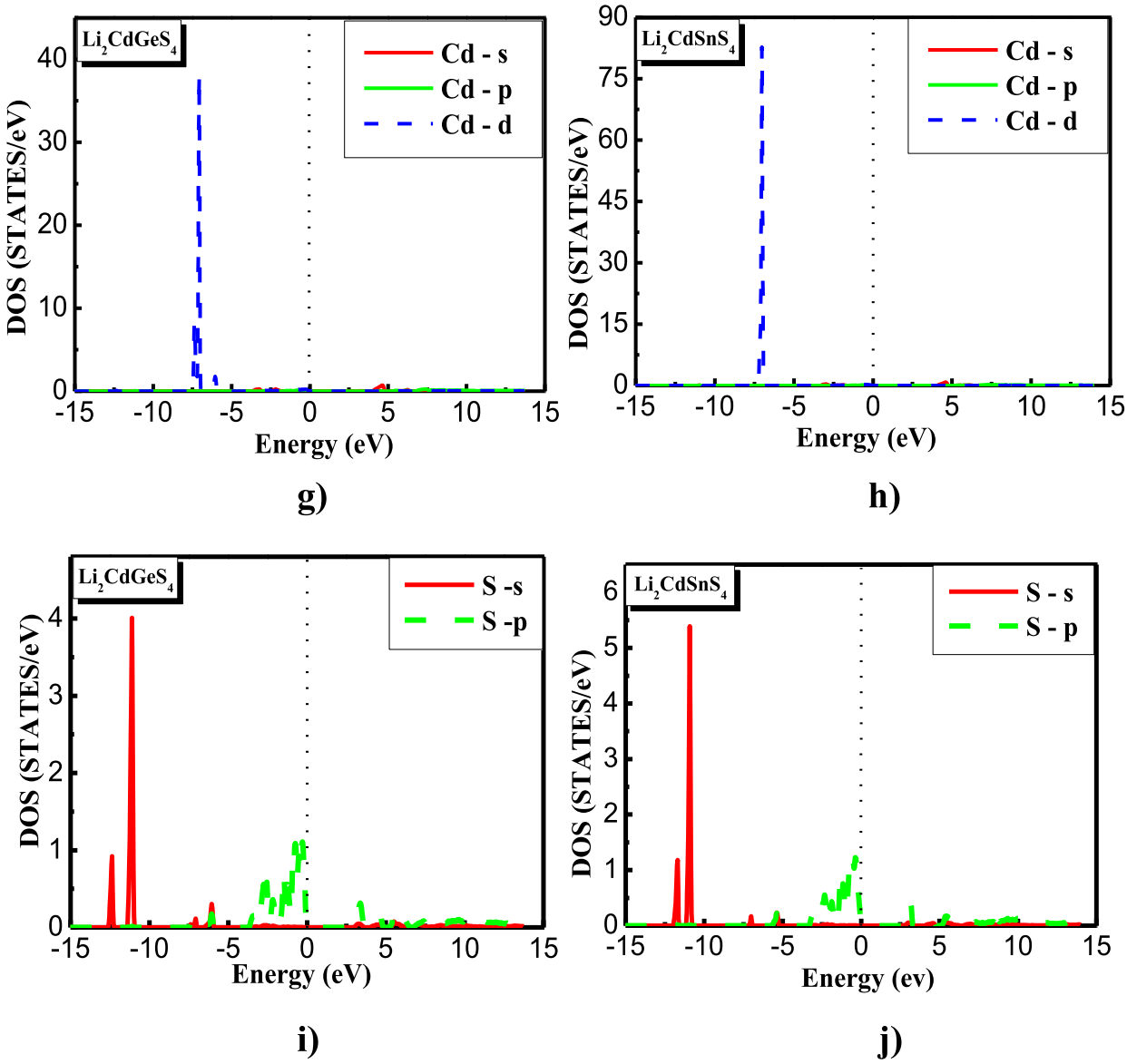

Figure 3. (Continued.)

the two compounds are reflected also in the absorption coefficient. Thus, the compounds have comparable absorption. Figures 5(a) and (b) depicts the calculated energy dependent absorption spectra for both DLSs. It is obvious from the absorption coefficient spectra that as the energy precedes the threshold energy, the absorption coefficient $I(\omega)$ increases with the increase of energy, reaching a maximum peak in the higher energy range from 8.0 to 13.60 eV. The maximum peaks are found at about 14 eV for the three components of the absorption coefficient. It is clear that our studied DLSs have a higher absorption in the ultraviolet region, which signifies that these materials are not transparent. In addition, there is a weak anisotropy among the three components, but a considerable anisotropy is found in the energy range between 6.0 and 8.0 eV for Li_2CdGeS_4 and from 6.5 to 13 eV for Li_2CdSnS_4.

The reflectivity spectra are presented in figures 5(c) and (d). It is interesting to observe that the considered DLSs illustrate reflectivity in the near ultraviolet region of about 40%, then it increases with energy and reaches a maximum value of about 70% at 13 eV. In addition, there is a considerable anisotropy among the three components, $R_{xx}(\omega)$, $R_{yy}(\omega)$ and $R_{zz}(\omega)$ from 4.0 eV to 10.0 eV, in particular for Li_2CdGeS_4 and from 4.0 eV to 12.0 eV for Li_2CdSnS_4.

Finally, we also extracted the refractive indexes, $n(\omega)$, as shown in figures 5(e)–(f). The static values of $n_{xx}(0)$, $n_{yy}(0)$ and $n_{zz}(0)$ are shown in table 4. As the energy increases the value of $n(\omega)$ increases, leading to a high transparency. Beyond the energy value of 6.0 eV, these graphs show a decrease in ultraviolet. It is found that in the infrared region, the refractive index increases with the increase of photon energy: the increase in the refractive index with the photon

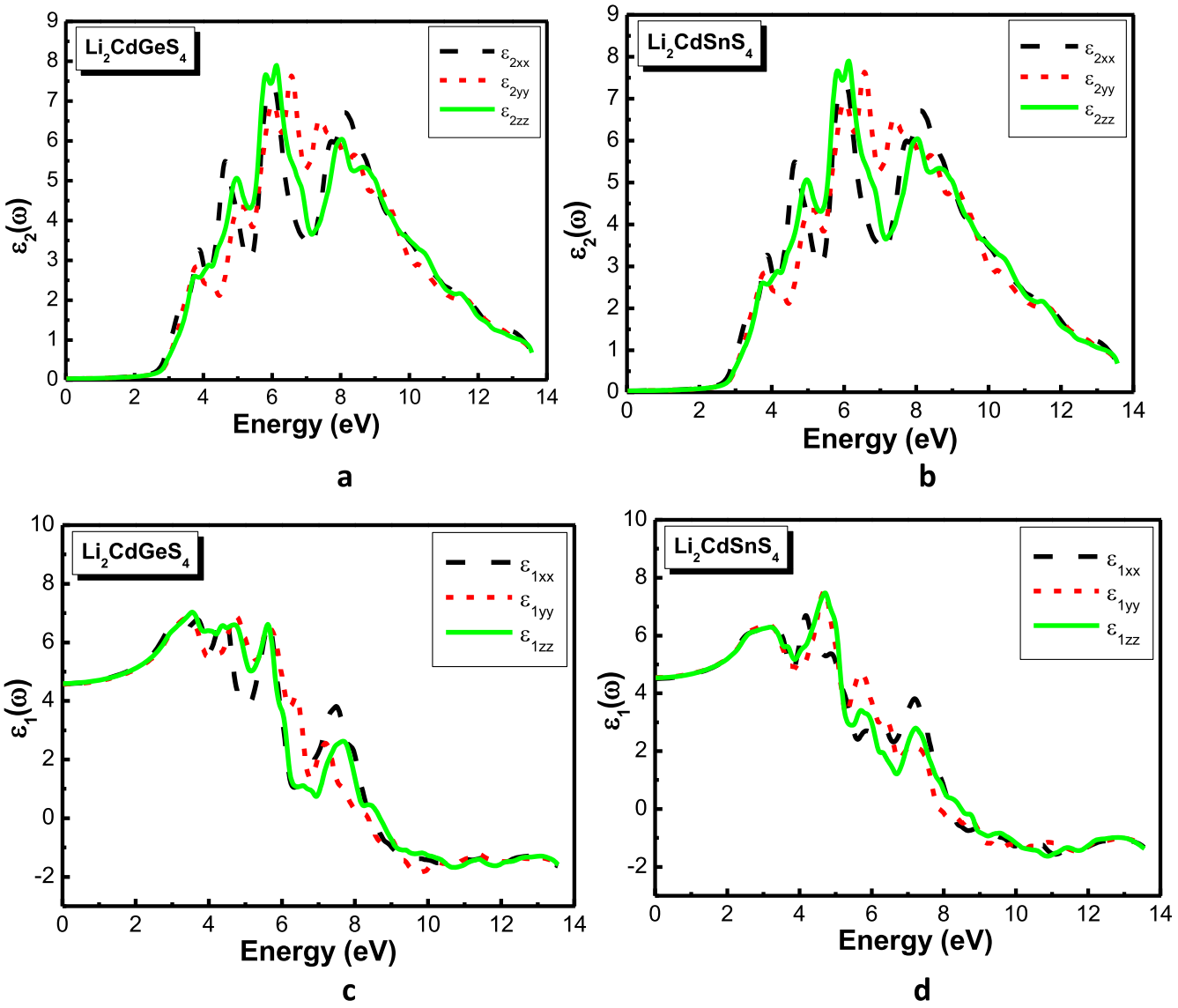

Figure 4. The imaginary part $\varepsilon_2(\omega)$ and the real parts $\varepsilon_1(\omega)$ of the dielectric functions of Li_2CdGeS_4 and Li_2CdSnS_4 diamond-like semiconductors.

energy shows normal dispersion behavior of the materials. Although the spectra of the refractive index still exhibits anisotropy.

3.4. Thermodynamic properties

Thermodynamic properties are very interesting, as they play a key role in understanding the thermal response of the crystals. Thermal properties including entropy, thermal expansion, heat capacity, and Grüneisen parameter are fundamental characteristics of materials. They provide important information such as interatomic interactions, anharmonicity of lattice vibrations, thermodynamic stability and the utility of materials for different applications. We present in the final section our results on the thermodynamic properties including the entropy *S,* the heat capacity C_v, the Debye temperature Θ_D of Li_2CdGeS_4 and Li_2CdSnS_4 using first-principles calculations within a quasi-harmonic approach which takes into consideration the phononic effects.

Since Li_2CdGeS_4 and Li_2CdSnS_4 compounds have a melting point of approximately 1090 K and 1196 K, respectively, the finite temperature properties are examined up to 1000 K. The pressure effects are investigated in the range of 0–8.0 GPa. Figures 6(a)–(b) shows the calculated equilibrium volumes at various temperatures for several values of the pressure. The overall volume of our crystals show a positive expansion on heating. Moreover, the trend of the variation of volume of Li_2CdGeS_4 with temperature is also similar to that of Li_2CdSnS_4. One can observe that the equilibrium volume increases sharply with increasing temperature,which indicates that Li_2CdGeS_4 and Li_2CdSnS_4 are soft materials.

The dependence of the bulk modulus on temperature is shown in figures 6(c)–(d). It is nearly a constant when $T < 100$ K, however, it decreases linearly with increasing temperature. The bulk modulus of Li_2CdGeS_4 and Li_2CdSnS_4 drops by 20.41% and 22.77%, respectively, from 0 to 1000 K. As can be seen, the bulk modulus of Li_2CdGeS_4 is higher

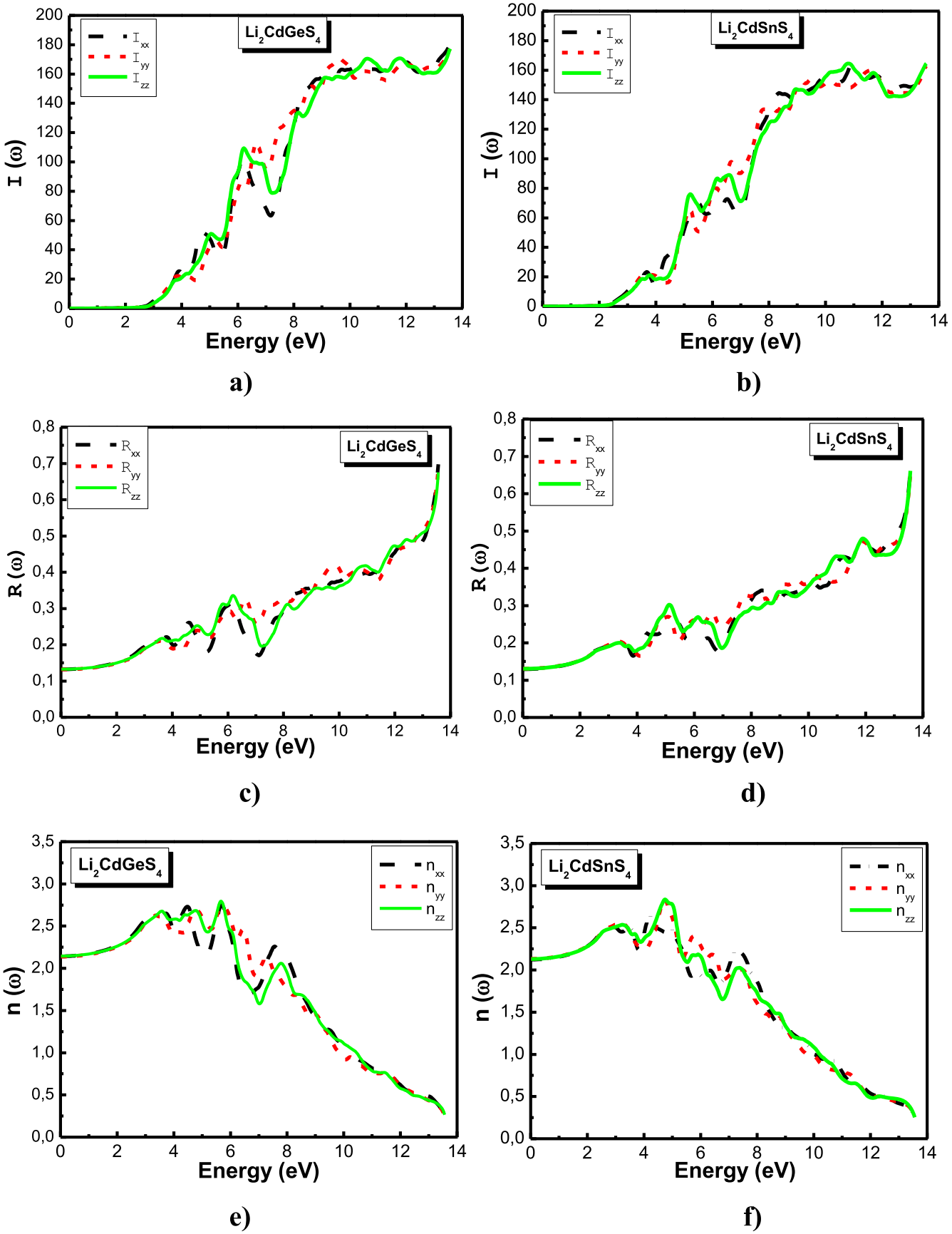

Figure 5. The absorption coefficient $I(\omega)$, reflectivity $R(\omega)$ and the refractive index $n(\omega)$ of Li_2CdGeS_4 and Li_2CdSnS_4 diamond-like semiconductors.

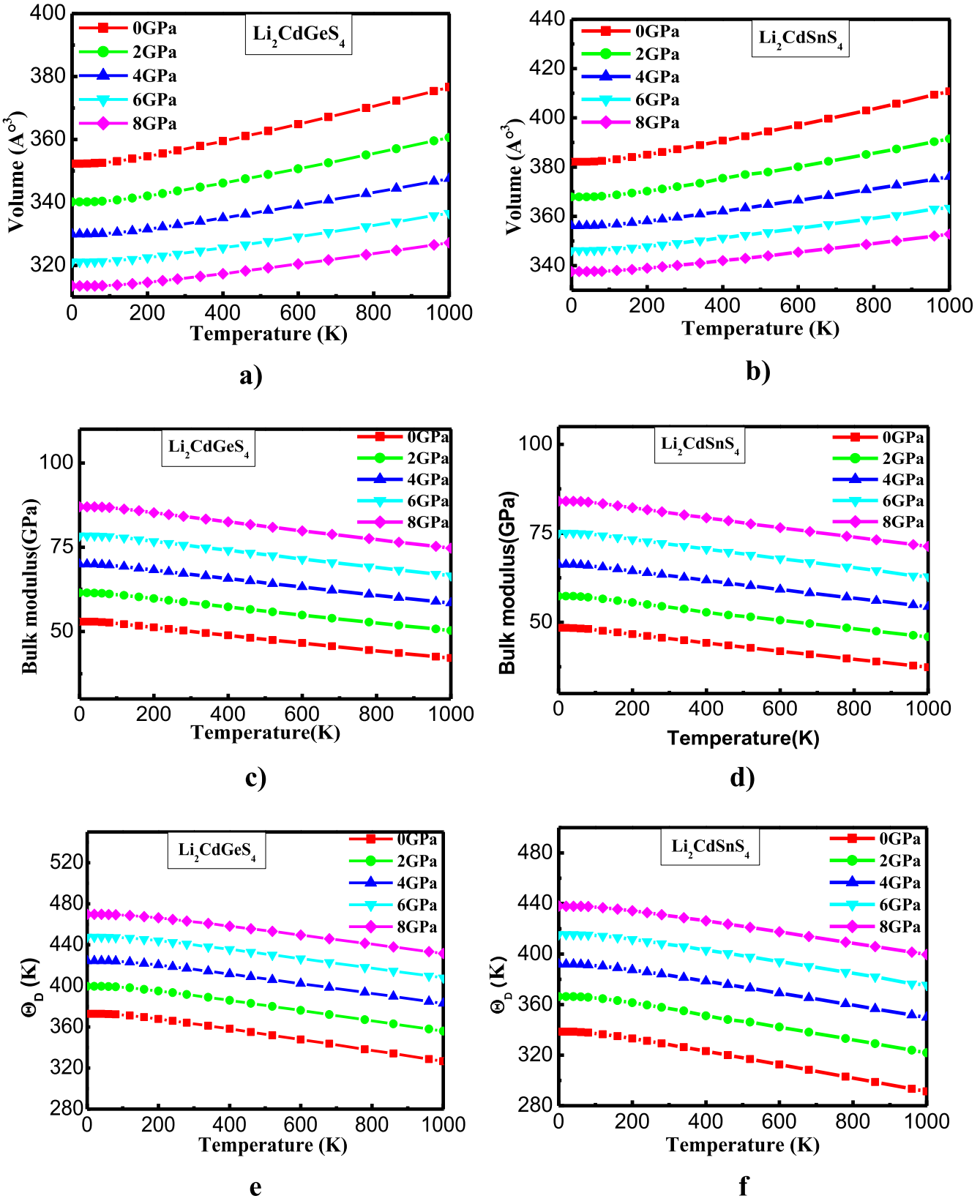

Figure 6. Variation of the cell volume, bulk modulus and Debye temperature Θ_D as a function of temperature of Li_2CdGeS_4 and Li_2CdSnS_4 diamond-like semiconductors at different pressures.

than that of Li_2CdSnS_4 in the whole temperature range. Considering the fact that the unit cell volume of Li_2CdGeS_4 is about 7.8% smaller than that of Li_2CdSnS_4 and the Ge-S bonding is stronger than Sn-S bonding, it is not surprising that Li_2CdGeS_4 possesses a higher bulk modulus. The bulk modulus calculated here is 52.90 GPa and 48.43 GPa for Li_2CdGeS_4 and Li_2CdSnS_4, respectively at 0 K and 0 GPa, which is in excellent agreement with our result (53.87 and 49.78 GPa) found within the LAPW-GGA method. The bulk modulus decreases smoothly with the temperature increasing which indicates that the compressibility increases with the increasing temperature. It is found that the bulk modulus of our compounds increases almost linearly with increasing pressure at a specific temperature, which shows that the cell volume undergoes a homologous variation.

The Debye temperature Θ_D is a basic physical feature, and is used to differentiate between low- and high-temperature regions for a crystal. If $T > \Theta_D$ we expect all modes to have energy k_BT, and if $T < \Theta_D$ one expects high-frequency modes to be frozen [55].

Figures 6(e)–(f) presents the calculated temperature dependent Debye temperature Θ_D of Li_2CdGeS_4 and Li_2CdSnS_4 at several pressures. The value of Debye temperature can represent interatomic binding forces thus it is related to the hardness of material, in general, a higher Debye temperature indicates a higher hardness which is not the case of our studied materials [56]. The dependence of Debye temperature on temperature at zero pressure shows a softening of the Li_2CdGeS_4 and Li_2CdSnS_4 crystals and the pressure can suppress such an effect.

Usually, a solid with high modulus and hardness will possess high Debye temperature. Accordingly, the Li_2CdGeS_4 and Li_2CdSnS_4 compounds are soft materials with an average Debye temperature, this confirms the results reported previously. One can see that at low pressure the Debye temperature Θ_D decreases smoothly when the temperature varies from 0 to 1000 K. However at a given temperature, it increases with pressure. So, we can conclude that the effect of temperature on the Debye temperature Θ_D is not as considerable as the effect of pressure on Θ_D.

Heat capacity is a key thermodynamic parameter, which gives important information on the vibrational properties of materials. It is possible to calculate specific heat at constant volume (C_v), and specific heat at constant pressure (C_p) using the following expression:

$$C_p = C_v(1 + \alpha\gamma T).$$

Our presently computed values of constant volume and pressure specific heat are plotted in figures 7(a)–(d). The constant pressure specific heat increases beyond the Dulong–Petit limit about 200 J mol^{-1} K^{-1} at high temperature, showing the role of anharmonicity at high temperatures. No experimental results are found for comparison.

As shown in figures 7(a)–(b), the temperature effect on C_p is much more significant than that of pressure. Unlike the C_p heat capacity curves, the C_v curves obey to the Dulong and Petit classical law [57] (200 J mol^{-1} K^{-1}). This is consistent with the equipartition theorem of classical mechanics: energy added to solids takes the form of atomic vibrations and both kinetic and potential energy is associated with the three degrees of freedom of each atom.

At sufficiently low temperatures, C_v is proportional to T^3 [58]. The low-T behavior can be explained by treating the quantum oscillators as collective modes in the solid (phonons) and showed that at low T, only low-energy, acoustic modes can be excited. At high temperatures while C_P follows a linear increase with the temperature increasing. For the entire temperature range and especialy above 200 K $C_p > C_v$ implies thermodynamic stability of the crystal. At zero pressure and ambient temperature, C_v and C_p are 185.66 (188.09) and 193.20 (196.74) J mol^{-1} K^{-1}, for Li_2CdGeS_4 (Li_2CdSnS_4), respectively. Furthermore, it can be seen that the entropy increases with increasing temperature and on the other hand it decreases with increasing pressure. In contrast to the heat capacity C_v at constant volume, the high temperature dependence of entropy S is sensitive to pressure, as shown in figures 8(a)–(b).

Thermal expansivity is the tendency of matter to change in volume in response to a change in temperature. It has been emphasized that there are certain difficulties associated with the measurement of the thermal expansion coefficient at high temperatures which leads to considerable uncertainties in the experimental values [59]. In order to study the influence of pressure and temperature on thermal expansivity of Li_2CdGeS_4 and Li_2CdSnS_4, calculations of the thermal expansion coefficients (volume expansion) α are performed with the quasi-harmonic Debye model. In real solids the forces between atoms are not truly harmonic. The potential energy varies with interatomic separation. The higher the temperature, the more phonons that are excited and the more pronounced the effects of anharmonicity. This leads to changes in the equilibrium separation of the atoms. The lattice therefore expands. Thermal expansion arises as a direct result of the asymmetrical dependence of potential energy on atomic separation, i.e. the anharmonicity. It is therefore not surprising that the variation of the coefficient of thermal expansion with temperature parallels that of the heat capacity.

Figures 8(c)–(d) presents the thermal expansion coefficient α of Li_2CdGeS_4 and Li_2CdSnS_4 as functions of both temperature and pressure. After a sharp increase, up to 300 K, α reaches a linear region in the temperature range of 300–1000 K. Furthermore, it is seen that it decreases rapidly as the pressure increases. The temperature effect becomes less important indicating that the anharmonic effects are important at low pressures and high temperatures for the materials under consideration. Table 5 contains a selection of the thermal properties predicted for Li_2CdGeS_4 and Li_2CdSnS_4 at 0 K and room temperature. The principal aspect from our results is the close similarity of both compounds. The thermal expansion coefficient of Li_2CdGeS_4 is lower than that of Li_2CdSnS_4, wich is consistent with the fact that Li_2CdGeS_4 possesses a higher bulk modulus and lower volume reduction when compressed.

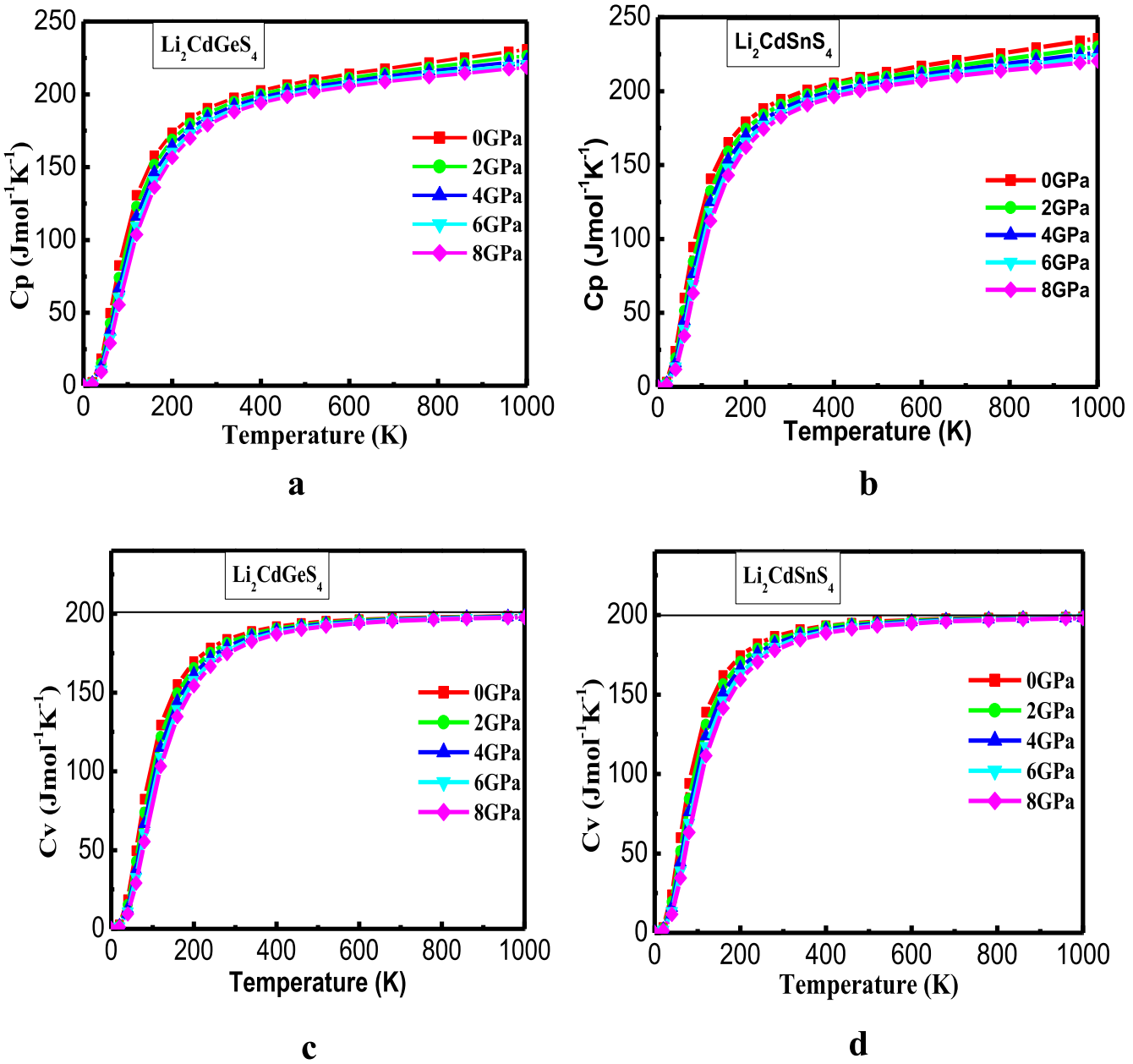

Figure 7. Variation of the heat capacities C_p and C_v versus temperature of Li_2CdGeS_4 and Li_2CdSnS_4 diamond-like semiconductors at different pressures.

4. Conclusions

We have carried out DFT calculations of the structural, electronic, optical and thermodynamic properties of Li_2CdGeS_4 and Li_2CdSnS_4 compounds. The phases of both compounds are diamond-like with the tetrahedra pointing in the same direction along the *c*-axis. The bond angles and bond lengths are calculated. It is noted that replacing Ge by Sn leads to a long bond length.

The ground state properties like equilibrium volumes, bulk modulus and its first derivative *B*' obtained in our study agree with the available experimental and theoretical data. Electronic band structure calculations show a direct energy gap of 2.79 and 2.42 eV, which suggests that the Li_2CdGeS_4 and Li_2CdSnS_4 compounds are appropriate for applications in optoelectronic devices. Replacing Ge by Sn is analyzed and discussed in detail for the electronic structure and the nature of chemical bonds and thermal properties. It was discovered that the band gap of Li_2CdGeS_4 material could be widened to 2.79 eV, when replacing Sn by Ge atom. To fully explain and understand the origin of the trend in band gap energy, in addition to bond distance and electronegativity, we calculated the DOS to see which orbitals contribute to the states around the band gap. Therefore, we concluded that the bonding behavior of Li_2GeCdS_4 is a coexistence of ionic and covalent nature.

Moreover the complex dielectric function, refractive index, extinction coefficient, absorption coefficient, reflectivity are also calculated, which show significant optical

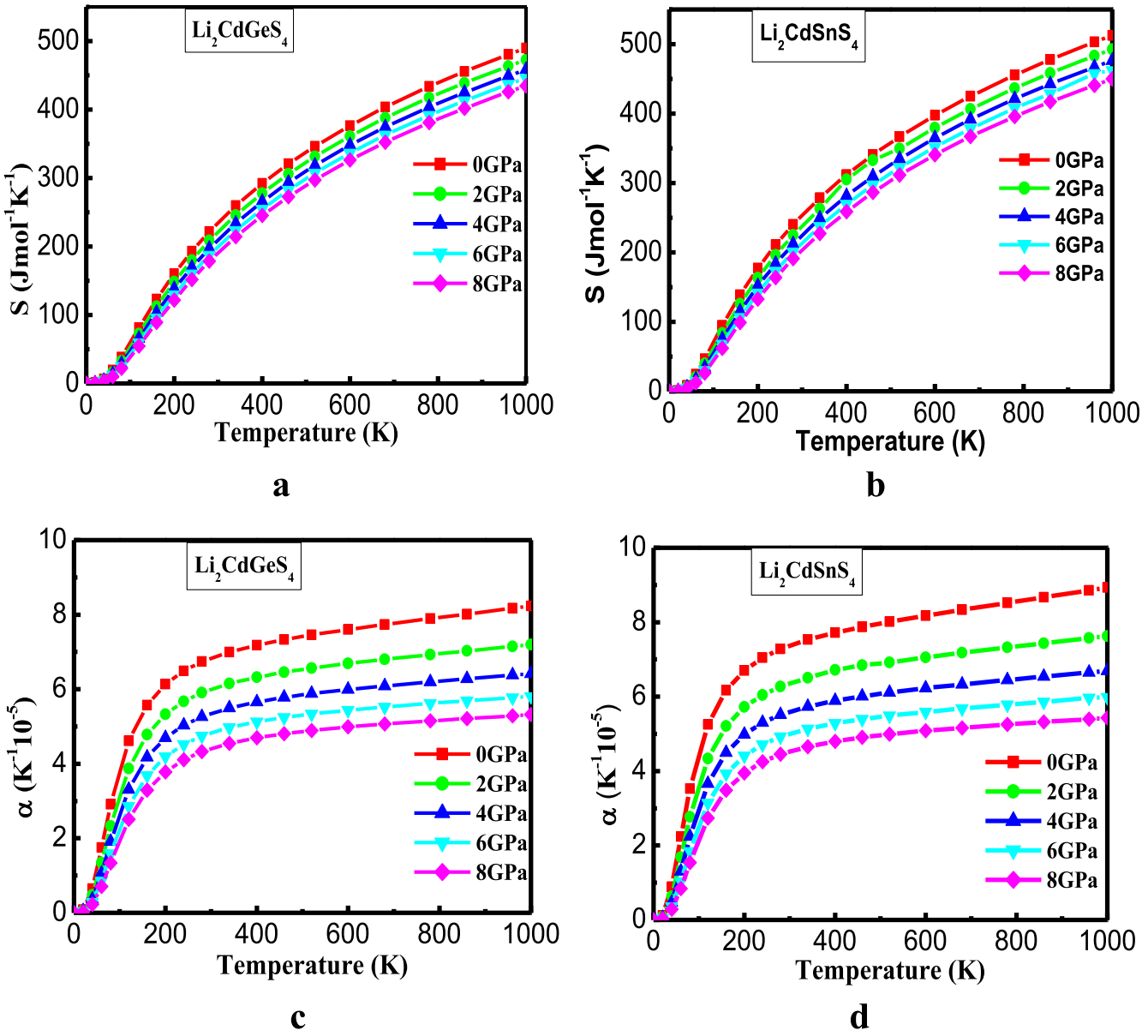

Figure 8. Variation of the entropy and the volume expansion coefficient as a function of temperature of Li_2CdGeS_4 and Li_2CdSnS_4 diamond-like semiconductors at different pressures.

Table 5. Thermal parameters at 0 and 300 K: thermal expansion coefficient α; vibrational contribution to the volume and pressure constant heat capacities (C_v and C_p in J mol^{-1} K^{-1}); isothermal and adiabatic bulk moduli (B and B_S, in GPa); Debye temperature (Θ_D); and Grüneisen parameter (γ); and antropy S (J mol^{-1} K^{-1}).

Compounds	T	α	C_v	C_p	B	B_S	Θ_D	γ	S
Li_2CdGeS_4	0	0	0	0	52.90	52.90	365.04	1.98	0
	300	6.83	185.66	193.20	50.02	52.05	363.1	1.98	235.09
Li_2CdSnS_4	0	0	0	0	48.43	48.44	338.5	2.07	0
	300	7.37	188.09	196.74	45.43	47.52	328.28	2.07	253.93

anisotropies in the components of polarization directions (1 0 0), (0 1 0) and (0 0 1).

On the basis of the quasi-harmonic model within the first-principles study, the dependence of Debye temperature, the bulk modulus, entropy and heat capacity (C_v and C_p) on pressure and temperature are obtained in the whole pressure range from 0 to 8 GPa and temperatures below the melting temperature 1000 K and discussed. It is found that the bulk modulus rises with increasing pressure, and decreases with increasing temperature. In conclusion, the quasi-harmonic

approach predicts a relatively similar behaviour for both quaternary Li-containing diamond-like semiconductors Li_2CdGeS_4 and Li_2CdSnS_4.

These materials have polarizable M-S bonds resulting in high (NLO) coefficients; yet also have wider band gaps that may result in higher laser damage thresholds.

References

[1] Kanno R, Hata T, Kawamoto Y and Irie M 2000 *Solid State Ion.* **130** 97
[2] Goetzberger A, Hebling C and Schock H-W 2003 *Mater. Sci. Eng.* **R40** 1
[3] Hahn H, Frank G, Klingler W, Meyer A D and Störger G 1953 *Z. Anorg. Allg. Chem.* **271** 153
[4] Guo Q, Hillhouse H W and Agrawal R 2009 *J. Am. Chem. Soc.* **131** 11672
[5] Ford G M, Guo Q, Agrawal R and Hillhouse H W 2011 *Chem. Mater.* **23** 2626
[6] Fella M C, Uhl A R, Romanyuk Y E and Tiwari A N 2012 *Phys. Status Solidi* **A209** 1043
[7] Brant J A, Clark D J, Kim Y S, Jang J I, Zhang J-H and Aitken J A 2014 *Chem. Mater.* **26** 3045
[8] Ohmer M C, Pandey R and Bairamov B H 1998 *MRS Bull.* **23** 16
[9] Catella G C and Burlage D 1998 *MRS Bull.* **23** 28
[10] Davidyuk G E, Parasyuk O V, Semenyuk S A and Romanyuk Y E 2003 *Inorg. Mater.* **39** 919
[11] Liu M L, Chen I W, Huang F Q and Chen L D 2009 *Adv. Mater.* **21** 3808
[12] Shi X Y, Huang F Q, Liu M L and Chen L D 2009 *Appl. Phys. Lett.* **94** 122103
[13] Sevik C and Çağın T 2010 *Phys. Rev.* B **82** 045202
[14] Pearton S J, Abernathy C R, Norton D P, Hebard A F, Park Y D, Boatner L A and Budai J D 2003 *Mater. Sci. Eng.* **R40** 137
[15] Bachmann K J, Buehler E, Shay J L and Wernick J H 1975 *U. S. Publ. Pat. Appl.* B **382** 021
[16] Parthé E, Yvon K and Dietch R H 1969 *Acta Crystallogr. Sec.* B **25** 1164
[17] Schäfer W and Nitsche R 1974 *Mater. Res. Bull.* **9** 645
[18] Moodie A F and Whitfield H J 1986 *Acta Crystallogr. Sec.* B **42** 236
[19] Roque Infante E, Delgado J M and López Rivera S A 1997 *Mater. Lett.* **33** 67
[20] Parasyuk O V, Gulay L D, Romanyuk Y E and Olekseyuk I D 2002 *J. Alloy compd.* **334** 143
[21] Quintero M, Barreto A, Grima P, Tovar R, Quintero E, Porras G S, Ruiz J, Woolley J C, Lamarche G and Lamarche A-M 1999 *Mater. Res. Bull.* **34** 2263
[22] Parasyuk O V, Gulay L D, Romanyuk Y E and Piskach L V 2001 *J. Alloy compd.* **329** 202
[23] Li Y, Fan W, Sun H, Cheng X, Li P and Zhao X 2011 *J. Phys.: Condens. Matter* **23** 225401
[24] Li X, Peng W and Fu H 2013 *J. Alloy compd.* **581** 867
[25] Devi M S and Vidyasagar K 2002 *J. Chem. Soc., Dalton Trans.* **9** 2092
[26] Lekse J W, Moreau M A, McNerny K L, Yeon J, Halasyamani P S and Aitken J A 2009 *Inorg. Chem.* **48** 7516
[27] Wei L, Fan W, Li Y, Zhao X and Yang L 2013 *J. Solid. State. Chem.* **201** 48
[28] Parasyuk O V, Olekseyuk I D, Piskach L V, Volkov S V and Pekhnyo V I 2005 *J. Alloy compd.* **399** 173
[29] Davydyuk G Y, Parasyuk O V, Romanyuk Y E, Semenyuk S A, Zaremba V I, Piskach LV, Kozioł J J and Halka V O 2002 *J. Alloy compd.* **339** 40
[30] Brunetta C D, Karuppannan B, Rosmus K A and Aitken J A 2012 *J. Alloy compd.* **516** 65
[31] Jackson A G, Ohmer M C and LeClair S R 1997 *Infrared Phys. Technol.* **38** 233
[32] Chapuis G and Niggli A 1972 *Acta Crystallogr. Sec.* B **28** 1626
[33] Blaha P, Schwarz K, Madsen G K H, Kvasnicka D and Luitz J 2001 *WIEN2K, An Augmented Plane Wave + Local Orbitals Program for Calculating Crystal Properties, Karlheinz Schwarz* (Wien, Austria: Techn. Universitat) ISBN3-9501031-1-1-2
[34] Kohn W and Sham L J 1965 *Phys. Rev.* A **140** 1133
[35] Perdew J P, Burke S and Ernzerhof M 1996 *Phys. Rev. Lett.* **77** 3865
[36] Engel E and Vosko S H 1993 *Phys. Rev.* B **47** 13164
[37] Jepson O and Anderson O K 1971 *Solid State Commun.* **9** 1763
[38] Liu Q J, Liu Z T, Feng L P and Tian H 2010 *Solid State Sci.* **12** 1748
[39] Saniz R, Ye L H, Shishidou T and Freeman A J 2006 *Phys. Rev.* B **74** 014209
[40] Holm B, Ahuja R, Yourdshahyan Y, Johansson B and Lundqvist B I 1999 *Phys. Rev.* **B59** 12777
[41] Wooten F 1972 *Optical Properties of Solids* (New York and London: Academic press)
[42] Otero-de-la-Roza A, Abbasi-Pérez D and Luaña V 2011 *Comput. Phys. Commun.* **182** 2232
[43] Otero-de-la-Roza A and Luaña V 2011 *Comput. Phys. Commun.* **182** 1708
[44] Peng W, Li X and Du J 2013 *Mater. Trans.* **54** 2167
[45] Bernert T and Pfitzner A 2006 *Z. Anorg. Allg. Chem.* **632** 1213
[46] Bernert T and Pfitzner A 2005 *Z. Kristallogr.* **220** 968
[47] Parasyuka O V, Romanyuka Y E and Olekseyuk I D 2005 *J. Cryst. Growth* **275** 159
[48] Shannon R D 1976 *Acta Crystallogr. Sec.* A **32** 751
[49] Emsley J 1997 *J. The Elements* (Oxford: Oxford University Press)
[50] Parasyuk O, Kityk I V, Kamarudin H and Chmiel M 2012 *Spectrochimica Acta Part* A **93** 274
[51] Charifi Z, Baaziz H, El Haj Hassan F and Bouarissa N 2005 *J. Phys.: Condens. Matter* **17** 4083
[52] Ichikawa T, Maeda T, Matsushita H and Katsui A 2000 *J. Adv. Sci.* **12** 99
[53] Reshak A H, Nouneh K, Kityk I V, Bila J, Auluck S, Kamarudin H and Sekkat Z 2014 *Int. J. Electrochem. Sci.* **9** 955
[54] Pauling L 1960 *The Nature of the Chemical Bond* 3rd edn (Ithaca: Cornell University Press)
[55] Christman J R 1988 *Fundamentals of Solid State Physics* (New York: Wiley)
[56] Ravindran P, Fast L, Korzhavyi P A, Johansson B, Wills J and Eriksson O 1998 *J. Appl. Phys.* **84** 4891
[57] Petit A T and Dulong P L 1819 *Ann. Chim. Phys.* **10** 395
[58] Debye P 1912 *Ann. Phys.* **39** 789
[59] Anderson O L and Zou K 1989 *Phys. Chem. Miner.* **16** 642